Simultaneously spatiotemporal gene expression and chromatin accessibility for mouse brain development

Fuqing Jiang[1,#], Xin Zhou[1,#], Yingying Qian[2,#], Li Wang[2], Qingmei Shen[1], Fangfang Qu[1], Guizhong Cui[1], Kai Chen[3], Guangdun Peng[1,2,4]

1Center for Cell Lineage and Atlas, Bioland Laboratory (Guangzhou Regenerative Medicine and Health Guangdong Laboratory), Guangzhou 510005, China

2Center for Cell Lineage and Development, CAS Key Laboratory of Regenerative Biology, Guangdong Provincial Key Laboratory of Stem Cell and Regenerative Medicine, GIBH-HKU Guangdong-Hong Kong Stem Cell and Regenerative Medicine Research Centre, University of Chinese Academy of Sciences, Guangzhou Institutes of Biomedicine and Health, Chinese Academy of Sciences, Guangzhou 510530, China

3Yunnan Key Laboratory of Primate Biomedical Research, Institute of Primate Translational Medicine, Kunming University of Science and Technology, Kunming, Yunnan 650500, China

4Institute for Stem Cell and Regeneration, Chinese Academy of Sciences, Beijing 100101, China

#: equal contribution

*: corresponding author, email: peng_guangdun@gibh.ac.cn

Brain are complex biological tissues which function relies on coordinated anatomical and molecular structure comprised by a large number of specialized cells. The spatial architecture of brain which is key to the understanding of its physiological and pathological significance is formed during embryo development. However, the molecular basis for discrete neuroanatomical domains particularly in the context of spatial organization of the brain is inadequate. Here, we introduced Spatial-ATAC-RNA-seq by crisscross indexing (SPARC-seq), a method for parallel profiling of gene expression and chromatin accessibility with spatial information retained in developing mouse brain. Our study has established a direct means to spatially determine the coordination between chromatin accessibility and transcriptome, identified the chromatin potential to define cell fate determination of brain structure, and uncovered spatiotemporal regulatory principles during mammalian brain development.

The brain is an enormously complex organ that composed of spatially organized and functionally interconnected neurons, glia and non-neural cells. An entry point in understanding brain development and function is to annotate the atlas of the brain by highly scalable and unbiased single-cell multi-omics approaches[1-4]. With the advent of spatial transcriptome technologies, the molecular cytoarchitecture of the brain has been unveiled in unprecedented detail[2, 5]. A complete description on spatially resolved transcriptome atlas for the developing and adult brain is on the horizon. However, one big challenge to define the building blocks of brain function lies in deciphering the complex regulatory network, e.g. the connection between chromatin modification and its transcription output, in forming the sophisticated tissue organization. Unfortunately, there is no existing method to simultaneously profile the gene expression and chromatin accessibility in the spatial context on a large scale, by which insightful gene regulatory interactions can be gained and is essential for dissecting the basis of neuroanatomical architecture.

To achieve a joint spatially resolved profiling of chromatin accessibility and gene expression, we devised a versatile Spatial-ATAC-RNA-seq by crisscross indexing platform (SPARC-seq) motivated by DBiT-seq design[6] and SHARE-seq methodology[7] (Fig. 1a and Supplementary Fig. 1a-c). In SPARC-seq, we modified the flow of microchannels and sealing slabs to facilitate a leakage-prevent and minimized diffusion effect. Tn5 transposase assembled with read1 and read2 adaptor sequence is administrated to the tissue slide to label the open chromatin regions in situ. The tissue slide is refixed and mRNA is reverse transcribed using a poly (T) primer bearing an 10bp unique molecular identifier (UMI), read2 anchor sequence and a biotin tag. Next, the tissue section is put onto the microfluidic chip and a set of DNA barcode round1-i (i = 1 to 50) are flowed over the tissue surface through microchannel-guided delivery to ligate to the read2 anchors. A second set of DNA barcode round2-i are flowed over the same tissue surface through microchannels perpendicular to the tissue slides and are attached to the ends of the barcode 1 (Fig. 1b). These two rounds of ligation ensure a coordinated spatial barcoding to paired ATAC and mRNA molecules of at most 2500 grids (currently 50 μm in width, representing around 15-20 cells). Adjacent sections are stained to obtain a high-sensitivity anatomical structure for downstream imaging alignment. As a validation of leakage-free, Cy3 and Fam dyes are added with the two rounds of barcodes respectively. Additionally, these two dyes can form a 2D mosaic pattern on the tissue slides for coordinates calibration with H&E image (Fig. 1c).

We performed SPARC-seq on the fetal brain of E13.5, E15.5 and E18.5 mouse brain. For spatial ATAC-seq, a median of 16,472 to 34,730 unique fragments per grid was achieved after filtering low quality reads, of which between 30.7% to 45.6% fragments fell within peak regions, indicating a high coverage and low background. In comparison, the unique fragments per cell from 10x scATAC-

seq of E18.0 brain was 17,368 and the fraction of reads in peaks (FRiP) was 24.7%. A recently reported spatial-ATAC-seq based on similar platform had, on average, 36,303 unique fragments per gird in the same spatial resolution[8] (Fig. 1d and Supplementary Fig. 1g). Our SPARC-seq showed typical nucleosomal and subnucleosomal fragments distribution (Fig. 1f) and captured more transcription start sites (TSSs) compared to 10xscATAC-seq (Fig. 1g and Supplementary Fig. 1i). The TSSs enrichment score calculated among the unique nuclear fragments showed higher coverage of TSSs, compared to 10x scATAC-seq data. (Fig. 1e,g and Supplementary Fig. 1i). The fractions of read-pairs mapped to mitochondrial of each sample section were between 2.52% to 2.95%, which were slightly higher than 10xscATAC-seq platform but is reasonable due to the openness of the cells on tissue sections (Supplementary Fig. 1h). To further evaluate the quality of our spatial ATAC-seq data, we aggregated the chromatin profiles from 300 spatial grids of an E15.5 brain and we found it faithfully reproduced the bulk measurement of chromatin accessibility obtained from the ENCODE E15.5 forebrain data[9] (Fig. 1h). The correlations between biological replicates of serial tissue sections for spatial ATAC data were very high, suggesting the spatial-ATAC procedure in our joint-analysis is robust (Supplementary Fig. 1q).

Next, we evaluated the spatial RNA-seq performance during the co-measurement of both modalities. The tissue permeabilization and fixation is the key bottleneck to ensure technical compatibility. We introduced additional refixation by 4% formaldehyde before mRNA reverse transcription. We found this treatment increased the yield and quality of the spatial transcriptome data. The total number of UMIs and genes per gird were comparable or even better than DBiT-seq in the same 50μm resolution[6] (Fig. 1i,j). Our aggregated DNA accessibility and RNA reads profiles of the same E15.5 mouse brain section showed that the RNA reads were located in the 3' end and the peaks of DNA accessibility were located in the TSS region of the same gene, indicating we could deduce the chromatin-gene expression relationships in cells of the same spatial locations (Fig. 1k).

Leveraging the two modalities of epigenome and transcriptome, we assessed the ability of SPARC-seq to identify the spatial architectures and query the cell relationship between chromatin accessibility and gene expression at individual stages using the ArchR and Seurat package[10, 11]. We found that both the spatial-ATAC and spatial-RNA-seq successfully delineates the anatomical structures and molecular activities. Using E15.5 mouse brain as an example (Supplementary Fig. 2a-l and 2i-m), we identified 14 ATAC clusters and 15 RNA clusters with their enriched chromatin or expression features in 11 major histological and cell types compositions, including thalamus, midbrain, hindbrain, muscle, skin and etc. The ATAC signal captured spatially resolved chromatin openness. For example, Satb2, a key regulator in mouse and human

cerebral cortex developing, was found highly accessible in mantle zone of dorsal pallium[12] (DPallm) (Supplementary Fig. 2f,g and 3a,d). Nr2e1, another key neocortex development regulator, was found highly accessible (represented by gene score value) in ventricular zone of dorsal pallium (DPallv)[13] (Supplementary Fig. 2i,j and 3b). Zic1, a key TF in brain development was found highly accessible in hindbrain region[14] (Supplementary Fig. 3c,e,f). The chromatin accessibility activity correlates well with the gene expression revealed by the spatial-RNA-seq data and can be verified in the Allen Mouse Brain Atlas. Notably, although both measures revealed the same major spatial clusters (for example, DPallv and Muscle, Supplementary Fig. 5a-e), the spatial-RNA-seq characterized some gene expression clusters at higher resolution and vice versa. For example, the finer discrimination of cartilage and mesenchyme was revealed by RNA-seq in cluster 1 and 3, compared to ATAC cluster 11; while ATAC cluster 7 and 8 converge into RNA cluster 0 (Supplementary Fig. 5d). To further utilize the underlying chromatin accessibility data, we sought to examine cluster-specific transcription factor (TF) regulators with each cluster using deviations of TF motifs (Supplementary Fig. 3h,i). We found that key fate determination genes were frequently associated with TF motifs with a large number of peaks. For example, the enriched motifs in the peaks in E15.5 brain pallium correspond to Neurod transcription factors, consistent with their well-studied role in the cortical development[15] (Supplementary Fig. 3j). Myod1, which plays a role in myogenesis, was enriched in muscle cell clusters of the brain[16] (Supplementary Fig. 3k).

Having the co-assay of spatial-ATAC-seq and spatial-RNA-seq at E13.5, E15.5 and E18.5 stages, we sought to examine the comprehensive view of both parameters along the developmental process (Fig. 2a). We identified 17 ATAC clusters and 18 RNA-seq clusters with the combined dataset on one section of each stage (Fig. 2b,j) and replicate sections (Supplementary Fig. 6). Major anatomical structures can be readily delineated by ATAC-based clusters, which is similarly distinguished by RNA-based clusters (Fig. 2c-h,2l-n). The corresponding molecular annotations not only recapitulate the dynamic development of mouse brain cortex, but also reveal the coherent gene regulatory network. Shared ATAC or RNA module genes were involved in the functional layout of the interconnected brain regions (Fig. 2i,k). Notably, we also observed stage-specific signature clusters in both ATAC and RNA profiles, e.g. ATAC cluster 7 of thalamus representing later cortex development was missing at E13.5. ATAC cluster 15 of midbrain was missing at E18.5 for this region was not included in the section. Interestingly, only advanced stage cluster (RNA-seq cluster 17) was underrepresented at E13.5 for spatial RNA-seq profiles, suggesting a poised or priming chromatin accessibility featuring the cortex development (Fig. 2f-n).

Empowered by the unique ability of mapping the spatial ATAC with RNA-seq data, we anticipated that asynchronous cell fate determination may be illustrated through the integration of both modalities (See methods). We performed a co-embedding analysis of the spatial ATAC-RNA-seq data and identified 17 predicted group clusters with spatial distributions (Fig. 3a-f). The molecular annotation defined by the joint signatures showed a high level of agreement with current structure-based reference atlases and, importantly, also established new and finer subdivisions in several brain areas, including the isocortex and striatum (Fig. 3d-f). To connect the ATAC-clusters with RNA-clusters, we found that overall the pattern of chromatin diverged earlier than gene expression as revealed in the sankey plots (Fig. 3g), suggesting that the chromatin accessibility of spatially resolved cell fate determining genes may precede gene expression. To further understand the gene-regulatory mechanisms between ATAC and RNA clusters, we compared the differential activities of five clusters and then preformed marker gene analysis on spatial RNA data. Gene expression and accessibility of top markers (represented by genescore) have a good correlation with each other (Fig. 3h).

Finally, to recover the spatially organized developmental regulation during cortex expansion, we tracked the RNA and ATAC changes from venticular zone of pallium (Pallv) to mantle zone of pallium (Pallm) and ordered these grids in pseudo-time using ArchR (Fig. 3i,j). Spatially organized development trajectory was revealed by both ATAC and RNA (Supplementary Fig. 5h,i). Importantly, we identified many keynote genes which are involved in neurogenesis (Fig. 3k). For example, Pax6 and Satb2, both are required for stem cell maintenance in the CNS of human or mouse[17, 18], were expressed successively from the inner VZ to outer VZ (Fig. 3l), pointing to the feasibility to predict the spatiotemporal regulatory mechanisms by the joint-measurement of spatial ATAC and RNA profiles.

In conclusion, by jointly quantifying the chromatin accesibility and gene expression profile with spatial information retained, SPARC-seq reveals molecular architeture of brain cortex and regulatory control of tissue organization in time and space. Future opitimization to futher increase the spatial resolution, the scalability and layers of omics information will provide a more holistic understanding of biological mechnisms underlying the complex tissue organization.

References

1. Takei, Y. et al. Single-cell nuclear architecture across cell types in the mouse brain. *Science* **374**, 586-594 (2021).
2. La Manno, G. et al. Molecular architecture of the developing mouse brain. *Nature* **596**, 92-96 (2021).

3. Zhu, C. et al. Joint profiling of histone modifications and transcriptome in single cells from mouse brain. *Nature methods* **18**, 283-292 (2021).
4. Rosenberg, A.B. et al. Single-cell profiling of the developing mouse brain and spinal cord with split-pool barcoding. *Science* **360**, 176-182 (2018).
5. Ortiz, C., Carlen, M. & Meletis, K. Spatial Transcriptomics: Molecular Maps of the Mammalian Brain. *Annual review of neuroscience* **44**, 547-562 (2021).
6. Liu, Y. et al. High-Spatial-Resolution Multi-Omics Sequencing via Deterministic Barcoding in Tissue. *Cell* **183**, 1665-1681 e1618 (2020).
7. Ma, S. et al. Chromatin Potential Identified by Shared Single-Cell Profiling of RNA and Chromatin. *Cell* **183**, 1103-1116 e1120 (2020).
8. Deng, Y. et al. Spatial-ATAC-seq: spatially resolved chromatin accessibility profiling of tissues at genome scale and cellular level. *bioRxiv* (2021).
9. Consortium, E.P. An integrated encyclopedia of DNA elements in the human genome. *Nature* **489**, 57-74 (2012).
10. Granja, J.M. et al. ArchR is a scalable software package for integrative single-cell chromatin accessibility analysis. *Nature genetics* **53**, 403-411 (2021).
11. Hao, Y. et al. Integrated analysis of multimodal single-cell data. *Cell* **184**, 3573-3587 e3529 (2021).
12. Zhang, L. et al. Satb2 is required for the regionalization of retrosplenial cortex. *Cell death and differentiation* **27**, 1604-1617 (2020).
13. Schmouth, J.F. et al. Combined serial analysis of gene expression and transcription factor binding site prediction identifies novel-candidate-target genes of Nr2e1 in neocortex development. *BMC genomics* **16**, 545 (2015).
14. Twigg, S.R. et al. Gain-of-Function Mutations in ZIC1 Are Associated with Coronal Craniosynostosis and Learning Disability. *American journal of human genetics* **97**, 378-388 (2015).
15. Singh, A. et al. Tcf12 and NeuroD1 cooperatively drive neuronal migration during cortical development. *Development* **149** (2022).
16. Rovito, D. et al. Myod1 and GR coordinate myofiber-specific transcriptional enhancers. *Nucleic acids research* **49**, 4472-4492 (2021).
17. Zeisel, A. et al. Brain structure. Cell types in the mouse cortex and hippocampus revealed by single-cell RNA-seq. *Science* **347**, 1138-1142 (2015).
18. Xu, Y. et al. PAUPAR and PAX6 sequentially regulate human embryonic stem cell cortical differentiation. *Nucleic acids research* **49**, 1935-1950 (2021).

Author contributions

G.P., and J.F. designed the study. J.F., X. Z., Y.Q., L.W. and S.Q. performed the experiments. J.F. analyzed the data with help from F.Q. and G.C. K.C. provided reagents and suggestions. J.F. and G.P. wrote the manuscript with the help of others.

Acknowledgments

This work was supported in part by National Key R&D Program of China (2018YFA0107200, 2018YFA0801402), the "Strategic Priority Research Program" of the Chinese Academy of Sciences, Grant No. (XDA16020404), National Natural Science Foundation of China (31871456 and 32100483), Guangdong Basic and Applied Basic Research Foundation (2019B151502054, 2019A1515110985 and 2020A1515110517), Frontier Research Program of Bioland Laboratory (Guangzhou Regenerative Medicine and Health Guangdong Laboratory, 2018GZR110105013), Jiazi Research Innovative Project of Bioland Laboratory (2019GZR110108001), Science and Technology Planning Project of Guangdong Province (2020B1212060052). We thank Patrick Tam for discussions and critical reading of this study.

Figure information

Fig. 1 | SPARC-seq: design, workflow and data quality. a, The composition of microfluidic devices used in this article, including PDMS slab, barcode inlets, acrylic clamp and suction device. **b**, SPARC-seq workflow. The tissue section was first subjected to Tn5 tagmentation, followed by reverse transcription (RT) and finally two rounds of barcode (50 kinds each) ligation on chip. R1, Read1 adaptor. R2, Read2 adaptor. **c**, Verification of leakage or diffusion by Cy3 and Fam dye. **d-g**, Comparison of FRiP value (d), TSS Enrichment value (e), insert size distribution (f) and TSS enrichment profile (g) between SPARC-seq and 10x scATAC-seq, S1, Section1. S2, Section2. **h**, Aggregate spatial ATAC peak profile compared to published profiles of ATAC-seq in E15.5 mouse brain. **i-j**, Comparison of UMIs (i) and genes (j) per pixel between SPARC-seq and DBiT-seq. **k**, Comparison of aggregate spatial ATAC peak profiles, spatial RNA reads profiles and ENCODE profiles of ATAC-seq in E15.5 mouse brain.

Fig. 2 | Spatial chromatin accessibility and gene expression mapping for mouse brain development at E13.5, E15.5 and E18.5. a, Overview of the sampled embryonic time points (Top) and H&E image from an adjacent tissue section (bottom). **b**, Spatial ATAC UMAP visualization of combined different mouse brain development stages. **c-e**, Anatomic annotation of major tissue regions based on the H&E image for different mouse brain development stages, E13.5 (c), E15.5 (d), E18.5 (e). **f-h**, Unsupervised clustering of mouse brain sections across E13.5 (f), E15.5 (g), E18.5 (h) for spatial ATAC. **i**, Heatmap of spatial ATAC marker genes across all clusters. **j**, UMAP visualization of spatial-RNA-seq of combined mouse brain development stages. **k**, Heatmap of spatial RNA marker genes across all clusters. **l-n**, Unsupervised clustering of mouse brain sections at E13.5 (l), E15.5 (m) and E18.5 (n) for spatial RNA-seq.

Fig. 3 | Integrated spatial chromatin accessibility and gene expression mapping for combined mouse brain development at E13.5, E15.5 and E18.5. a, UMAP display of combined Spatial RNA expression. **b**, Combined spatial ATAC clusters are projected to spatial RNA UMAP. **c**, Spatial ATAC clusters prediction to corresponding RNA clusters by ArchR. **d-f**, Spatial mapping of predicted clusters for different sections at E13.5 (d), E15.5 (e) and E18.5 (f). **g**, The cluster connective changes between ATAC, RNA and predicted clusters shown in sankey plots. **h**, Heatmap of top differential genes from spatial ATAC and RNA for selected clusters in predicted group. **i-j**, Cluster distributions of DPallv and DPallm along the pseudotime. **k**, Pseudotime heatmap of gene expression and genescore changes from DPallv to DPallm. DPallm, mantle zone of dorsal pallium. DPallv, ventricular zone of dorsal pallium. **l**, Spatial mapping of gene expression (RNA) and genescores (ATAC) for selected marker genes. In situ hybridization results of corresponding genes at E13.5, E15.5 and E18.5 mouse brain are from the Allen Mouse Brain Atlas.

Supplementary Figure 1. SPARC-seq design and data quality. a-c, Composition of spatial microfluidic chip for SPARC-seq analysis, including PDMS slab (a), Clamp and suction units (b), AutoCAD design of PDMS chip with 50μm channel width (c). **d-f**, Size distributions of ATAC library (d), cDNA amplicons (e) and cDNA library (f). **g-i**, Comparison of unique fragments value (g), percent mitochondrial value (h) and percent TSS fragments value (i) between SPARC-seq, 10x scATAC-seq and Spatial-ATAC-seq (shown as dash line[8]). **j-p**, Comparison of TSS enrichment scatterplot between different stage of mouse brain (l-q) from SPARC-seq and 10x scATAC-seq (k). **q**, Spearman correlation coefficient of bulk profiles from eight embryo mouse brain sections in this experiment.

Supplementary Figure 2. Spatial chromatin accessibility and gene expression mapping for E15.5 mouse brain. a-c, H&E image from an adjacent tissue section (a), UMAP clustering analysis (b) and spatial clusters of ATAC-seq projects to the brain section (c). **d**, Anatomic annotation of major tissue regions based on the H&E image and brain common coordinate framework. DPallm, mantle zone of dorsal pallium. DPallv, ventricular zone of dorsal pallium. **e**, Heatmap of spatial ATAC marker genes across all clusters. **f-k**, UMAP embedding (f, i) and spatial mapping (g, j) of gene scores for selected marker genes, and in situ hybridization of corresponding genes at E15.5 mouse brain are from the Allen Mouse Brain Atlas (h, k). **l-m**, UMAP unsupervised clustering analysis (l) and spatial anatomical distribution (m) of spatial RNA-seq. **n**, Heatmap of spatial RNA marker genes across all clusters, selected Gene Ontology (GO) terms are highlighted. **o-q**, UMAP embedding (o) and spatial mapping (p) of gene expression for selected marker genes, and in situ

hybridization of corresponding genes at E15.5 mouse brain are from the Allen Mouse Brain Atlas (q).

Supplementary Figure 3. Spatial chromatin accessibility for E15.5 mouse brain. a-c, Genome browser tracks for selected marker genes in different clusters. **d-g**, UMAP embedding (e) and spatial mapping (d, f) of gene scores for selected marker genes. In situ hybridization of corresponding genes at E15.5 mouse brain are from the Allen Mouse Brain Atlas (g). **h**, Heatmap of enriched spatial ATAC marker peaks across all clusters. **i**, Heatmap of enriched motifs within the marker peaks of each cluster. **j-k**, Tn5 bias-adjusted transcription factor footprints for selected motifs.

Supplementary Figure 4. Spatial gene expression for E15.5 mouse brain. a-b, Spatial expression UMIs (a) and genes (b) projected onto the H&E image. **c-f**, UMAP embedding (c, e) and spatial mapping (d, f) of gene scores for selected marker genes. **g-l**, UMAP embedding (g, j) and spatial mapping (h, k) of gene expression for selected marker genes, and in situ hybridization of corresponding genes at E15.5 mouse brain are from the Allen Mouse Brain Atlas (i, l).

Supplementary Figure 5. Integration of spatial chromatin accessibility and gene expression for E15.5 mouse brain. a, Spatial ATAC clusters are projected to spatial RNA UMAP. **b**, Spatial ATAC clusters are predicted to corresponding RNA clusters by integration in ArchR. **c**, Spatial mapping of predicted combined clusters. **d**, The connective cluster changes between ATAC, RNA and predicted clusters shown in Sankey plots. **e**, Heatmap of top differential genes from spatial ATAC and RNA for selected clusters in predicted group. **f-g**, Clusters distribution along the pseudotime. **h-i**, Spatial distribution of the pseudotime of RNA data (h) and ATAC data (i) of DPallv to DPallm. **j**, Pseudotime heatmap of gene expression and genescore changes from DPallv to DPallm.

Supplementary Figure 6. Replicate section (Section2) of spatial chromatin accessibility and gene expression mapping for mouse brain development at E13.5, E15.5 and E18.5. a-b, Spatial ATAC UMAP visualization of combined different mouse brain development stage. Colored by different sample sections (a) or different clusters (b). **c**, Heatmap of spatial ATAC marker genes across all clusters. **d-f**, H&E images from the adjacent tissue section at E13.5 (d), E15.5 (e) and E18.5 (f). **g-i**, Unsupervised clustering of mouse brain sections at E13.5 (g), E15.5 (h) and E18.5 (i) for spatial ATAC**. j-k**, Spatial RNA UMAP visualization of combined different development stages. Colored by different sample sections (h) or different clusters (k). **l**, Heatmap of spatial RNA marker genes across all clusters. **m-o**, Unsupervised clustering of mouse brain sections at E13.5 (m), E15.5 (n) and E18.5 (o) for spatial RNA.

Supplementary Figure 7. Comparison of spatial expression of selected genes with in situ hybridization data from Allen Mouse Brain Atlas. a-c, Spatial expression of predicted score for different sections at E13.5 (a), E15.5 (b) and E18.5 (c). **d-i**, Spatial mapping of gene expression (RNA) and gene scores (ATAC) for selected marker genes, and in situ hybridization of corresponding genes at E13.5, E15.5 and E18.5 mouse brain.

Table S1. DNA oligos used for PCR and preparation of sequencing library.

Table S2. DNA barcode sequence.

Methods

Mice

Mice were maintained in an animal facility approved by the Association for Assessment and Accreditation of Laboratory Animal Care (AAALAC), Guangzhou Institutes of Biomedicine and Health, Chinese Academy of Sciences. Procedures were approved by the Institutional Animal Care and Use Committees of GIBH (Institutional Animal Welfare Assurance Numbers N2019056). Normal brains were collected from wild-type mice of C57BL/6 mice at embryonic days 13.5-18.5. Mice of both sexes were used for the experiments.

Mice brain cryosection

Mouse brains at different embryonic stages were dissected, washed with 1x PBS, embedded in OCT (Leica Microsystems), and stored at -80°C for tissue sectioning. Pre-cool the cryostat in advance, set the temperature to -20 °C, and set the cutting thickness to 10 μm. Frozen blocks of OCT compounds were removed from cryo-embedding cassettes, and mouse brains from embryos at different stages were cut in sagittal planes, trimmed as needed, and attached to the metal stage of the OCT for cryosectioning. A piece of tissue is attached to each glass slice (188105, CITOTEST Scientific) and stored at -80°C.

H&E Staining

The adjacent frozen slide was warmed at room temperature for 10 min and fixed with 200μL 4% formaldehyde for 10 min. After decanting the formaldehyde, 200μL isopropanol was added to the slide and incubate for 2 min. After completely dried, the tissue section was stained with 200 μL hematoxylin (sigma) for 4 min and cleaned in distilled water. The section was then incubated in 200μL bluing reagent (sigma) for 1 min and rinsed in distilled water. At last, the section was stained with 200μL eosin (sigma) for 3 min and cleaned in distilled water.

Fabrication and assembly of microfluidic device

The device of microfluidic were fabricated using photo lithography. The thickness of the resistant and the channel width was 50 μm. The protocol of SU-8 photo lithography, development, and the hard baking was followed based on the manufacturer's (MicroChem) recommendations. The fabricated molds of SU-8 were used to reprint microfluidic resin masters. Last, for microfluidic chips fabrication, polydimethylsiloxane (PDMS) was prepared by mixing base and curing agent at a 10:1 ratio and then poured to the resin masters. After degassing, the PDMS was cured (80°C, 2h). PDMS slab was cut out after solidification and the inlet and outlet holes were punched for further use.

Transposome preparation

Unmodified Tn5 was purchased from manufacturer Vazyme (S601-01), and the transposome was assembled following manufacturer's guidelines. The oligos used for transposome assembly were as follows:

Tn5 Blocked_ME: /5Phos/C*T*G* T*C*T* C*T*T* A*T*A* C*A*/3ddC/

Tn5 Read 1:TCGTCGGCAGCGTCAGATGTGTATAAGAGACAG

Tn5 Pho_Read2: /5Phos/GTCTCGTGGGCTCGGAGATGTGTATAAGAGACAG

To evaluated the activity of the homemade Tn5, length distribution assay was performed using Qsep100 Bioanalyzer (Bioptic).

Preparing oligonucleotides for ligations

There were two rounds of barcode chip ligation in SPARC-seq, each round using a different 50 barcodes (Table S2). Hybridization oligos have a universal linker sequence that is partially complementary to specific barcode sequences. These strands anneal before organizing barcodes to generate DNA molecules with three distinct functional domains: 5' overhangs complementary to 5' overhangs on cDNA molecules or transposition DNA molecules (may be derived from RT primers, transposition adapters, or a previous round of barcodes), a unique tissue-specific barcode sequence and another 5' overhang that is complementary to the overhang on the DNA molecule to be ligated. To make 50 different round1 barcode mix in 96-well plate: add 25 μL 100 μM round 1 linker and 25 μL 50 different 100 μM barcodes to 50 different well and anneal the oligonucleotides by heating the plate to 95°C for 2 minutes and cooling to 20°C at a rate of about 1°C per minute. All oligonucleotides were dissolved in RNase-free water. The 50 different round2 barcode mix was prepared in the same way.

Fixation and blocking

Sagittal sections of mouse brains at different embryonic stages, freshly cut or cryopreserved, were equilibrated at room temperature for 10 min. The tissue was fixed with 1% formaldehyde (252549-500ML, Sigma) for 5 minutes and quenched with 125mM glycine for 5 min at room temperature. After fixation, the

tissue section was quickly dipped in 1X PBS. Then, 1% BSA containing 0.25% RNase inhibitor was added to the tissue slide for blocking at room temperature for 30 min. The tissue was then ready for transposition.

Transposition

The tissue section was permeabilized by Omni-ATAC buffer (10 mM Tris-HCl, pH 7.4; 10 mM NaCl; 3mM MgCl2; 0.1%Tween-20 (P9416-50ML, Sigma); 0.1%NP-40 (11332473001, Roche); 0.01% Digitonin (D141-500MG, Sigma); 1%PIC (05892970001, Roche)) plus 0.25% RNase inhibitor for 10 minutes at room temperature, then was washed with ATAC-RSB buffer (10 mM Tris-HCl pH 7.4; 10 mM NaCl; 3 mM MgCl2; 0.1% Tween-20; 0.25% RNase inhibitor) at room temperature for 5 min. And then the tissue section was washed by RNase free water for three times and air dried. 50 µL transposition buffer containing 0.25% RNase inhibitor (25 µL 2X TD buffer (20% Dimethylformamide; 20 mM Tris-HCl pH 7.4; 10 mM MgCl2); 19.4 µL 1X DPBS; 0.5 µL 10% Tween-20; 0.1 µL 5% Digitonin; 5 µL transposome) was added followed by incubation at 37°C for 30 minutes. To stop tagmentation, 100 µL TS buffer (20 mM EDTA;1 mM Spermidine) containing 0.25% RNase inhibitor were added after removing transposition buffer. The tissue slide was washed with ATAC-RSB buffer for 1 minute. And then the liquid was removed, the tissue slide was fixed with 4% formaldehyde at room temperature for 20 min and washed with ATAC-RSB buffer and 0.5x PBS.

Reverse transcription

Place tissue sections in a humidified box, and each tissue section was mixed with 45µL of RT mix (final concentration of 1x HiScript III buffer, 0.33M/µL RNase Inhibitor, 0.5x PBS,20M/µL HiScript III Reverse Transcriptase (R302, Vazyme), 500µM dNTP (18427088, Thermo) and 3.5µM RT primer with an affinity tag). The RT primer contains a poly-T tail, a Unique Molecular Identifier (UMI), a universal ligation overhang, and a biotin molecule. The RT reaction was done with regular procedure.

Ligation

200 µL of ATAC-RSB buffer containing 0.25% RNase inhibitor were added to the tissue area. The slide was gently washed by 200 µL of 1x NEBuffer 3.1. For the first round of ligation, longitudinal PDMS chips were attached in the area of interest and PDMS device were then clamped with an acrylic clamp. The brightfield image was taken with 4x objective (OLYMPUS microscope) for further alignment. 3 µL of Round1 barcode mix (1x T4 DNA ligase buffer, 16M/µL T4 DNA ligase (M0202L, NEB), 0.25M/µL RNase Inhibitor, NF-H2O, 1x NEBuffer 3.1, 5µM Cy3/Fam dye, 50µM round1 barcode mix) was added to each inlet well of the chip. The fluid was pulled over slowly with a syringe and the reaction was carried out at 37°C, 80rpm for 30min in a wet box. After the reaction, the Cy3 and 488 images were taken by fluorescence photography.

After discarded the ligation solution, the clamp and PDMS chip were removed and the tissue slide was washed by RNase free water. 200 μL of ATAC-RSB buffer was added to the tissue area. The second round of barcode ligation was similar to the first round.

Tissue digestion

50 μL 2x Lysis buffer (20mM Tris, pH8.0; 400mM NaCl; 100 mM EDTA ,pH8.0; 4.4% SDS; NF-H2O) and 10 μL proteinase K (20 mg/mL) (RT403-02, TIANGEN) was added to the slide and incubated for 10 min at room temperature. The lysate was further digested at 55 °C 2 h and collected into a 1.5 mL EP tube.

cDNA library preparation

RNA sequencing library was generated following the SHARE-seq protocol as previously reported with slight modifications. Briefly, the qPCR reaction was carried out at the following conditions: 95°C for 3 min, and then 30 thermal cycles at 98°C for 20 s, 67°C for 20 s and 72°C for 3 min. The PCR products were purified by 0.7X Kapa beads (A63882, BECKMAN COULTER) and dissolved in 15 μL RNase free water. cDNA concentration and fragment size distribution was determined by Qsep100 (Bioptic).

Spatial-RNA-seq library preparation

The cDNA library construction was performed according to the manufacturer's guidelines of TruePrep DNA Library Prep Kit V2 for Illumina (TD502, Vazyme).

Spatial-ATAC-seq library preparation

Zymo DNA Clean & Concentrator-5 (D4014, ZYMO research) was used to extract the genomic DNA in the supernatant retained after C1 beads purification, and eluted with 25μL of NF-H2O. 20 μL of the eluted purified product was then mixed with the PCR solution (2.5 μL 10 μM Ad1.01~Ad1.08 primer; 2.5 μL 10 μM P7 primer; 25 μL 2x NEBNext Master Mix (M0541, NEB)). Then, PCR was conducted with following the program: 58°C for 5 min, 72 °C for 5 min, 98 °C for 30 s, and then cycled 5 times at 98 °C for 10 s, 65°C for 10 s, and 72°C for 1 min. To determine additional cycles, 5 μL of the pre-amplified mixture was first mixed with the qPCR solution (0.5 μL10 μM Ad1.01~Ad1.08 primer; 0.5 μL 10 μM P7 primer; 1μl 20x SYBR Green (31000, BIOTIUM); 10μL 2x NEBNext Master Mix; 2 μL NF-H2O). Then, qPCR reaction was carried out at the following conditions: 98°C for 30 s, and then 30 cycles at 98°C for 10 s, 65°C for 10 s, and 72°C for 1 min. Finally, the remainder 45μL of the pre-amplified DNA was amplified by running the required number of additional cycles of PCR (cycles needed to reach 1/3 of saturated signal in qPCR). The PCR products were further purified by 1X Kapa beads and dissolved in 15 μL RNase free water.

Sequencing strategy

Both libraries were sequenced on an MGI-seq 2000 sequencer (BGI company) using a pair-end mode. cDNA library was sequenced with read1 75bp, read2 10bp, index5 8bp and index7 50bp. ATAC library was sequenced with read1 75bp, read2 75bp, index5 8bp and index7 50bp.

Spatial-RNA-seq processing

The read2 sequence was processed by extracting the UMI, round1 barcode and round2 barcode. The processed read 1 was trimmed, mapped against the mouse genome (mm10), demultiplexed and annotated (Gencode release VM23) using a custom script, which generated the digital gene expression matrix for down-stream analysis. To filter the data in non-tissue regions, microscope images with two channels were used to identify the pixel locations with manual selection using Adobe Photoshop and generated a mask picture which tissue region was filled with white color while non-tissue region was filled with black color. Then we can use a custom Matlab scripts to get the filtered barcode location. Normalization and variance stabilization of transcriptome data for each pixel with regularized negative binomial regression was performed using ‘‘SCTransform,’’ a module in Seurat v4.0. To visualize data, the top 3,000 variable genes were projected into 2D space by UMAP. Spatial clusters were plotted to adjacent HE stained tissue by custom R script according to the relationship of barcode and location (round1 barcode as column and round2 barcode as row).

Spatial-ATAC-seq processing

The sequences were transformed to Cell Ranger ATAC format using a custom python script from Spatial-ATAC-seq[8]. Resulting fastq files were aligned to mouse genome (mm10) and counted using Cell Ranger ATAC v2.0. The fragment files were generated for downstream analysis. Data filtering follows the same procedure with Spatial-RNA-seq processing. The filtered fragments file was then read into ArchR as a tile matrix in 5kb genome binning size, and pixels not on tissue were removed based on the metadata file generated from the previous step. Data normalization and dimensionality reduction was performed using Latent Semantic Indexing (LSI) of default parameters, followed by graph clustering and Uniform Manifold Approximation and Projection (UMAP) embeddings (nNeighbors = 30, metric = cosine, minDist = 0.5). Marker regions/genes for each cluster were identified using the getMarkerFeatures and getMarkers function in ArchR (testMethod = "wilcoxon", cutOff = "FDR <= 0.05"), and gene scores imputation was implemented with addImputeWeights function for data visualization. Peaks were called using the MACS2. Motif enrichment and motif deviations were calculated using peakAnnoEnrichment and addDeviationsMatrix function in ArchR. GO enrichment analysis was implemented using the clusterProfiler package (qvalueCutoff = 0.05). To map the data back to the tissue section, it’s the same with Spatial-RNA-seq processing.

Integrative data analysis

For Spatial-RNA-seq, different development embryo brain data integration was performed using ‘‘FindIntegrationAnchors’’ and “IntegrateData”, a module in Seurat v4.0. For Spatial-ATAC-seq, the data was integrated by using “RunHarmony” a mudule in Harmony v0.1.0. For SPARC-seq data integration, the Spatial-RNA-seq profiles were added to Spatial-ATAC-seq profiles using addGeneIntegrationMatrix function in ArchR.

Data quality comparison with other methods

E15.5 mouse forebrain bulk ATAC-seq data was downloaded from ENCODE and E11.0 whole mouse DBiT-seq data (50μm resolution) was downloaded from GSE137986. Besides, in situ hybridization and expression images were downloaded from Allen Mouse Brain Atlas.

Fig. 1

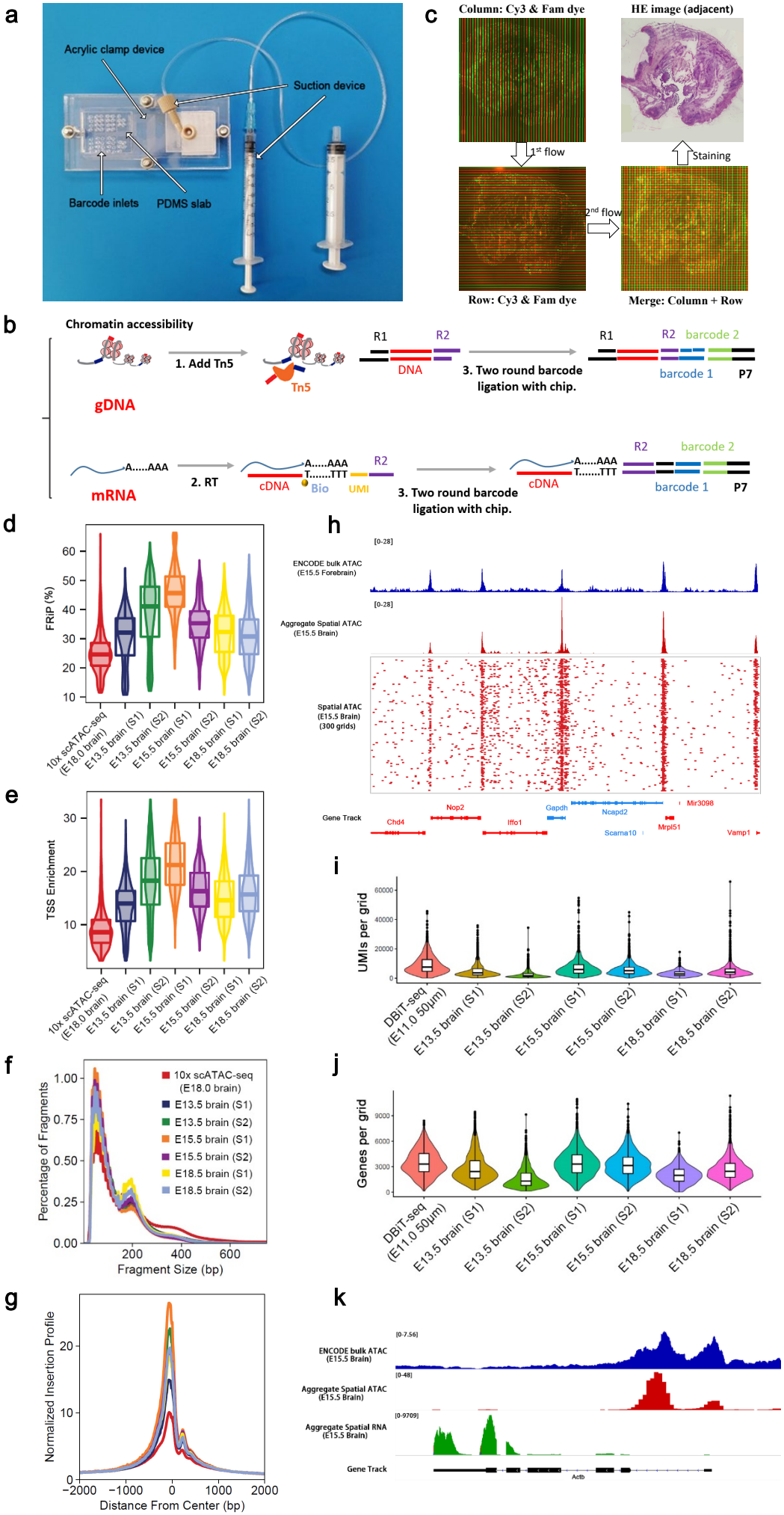
a
Acrylic clamp device
Suction device
Barcode inlets
PDMS slab
c
Column: Cy3 & Fam dye
HE image (adjacent)
1st flow
Staining
2nd flow
Row: Cy3 & Fam dye
Merge: Column + Row
b
Chromatin accessibility
1. Add Tn5
Tn5
gDNA
R1
R2
DNA
3. Two round barcode ligation with chip.
barcode 2
barcode 1
P7
mRNA
A.....AAA
2. RT
cDNA
T.....TTT
Bio
UMI
d
FRiP (%)
10x scATAC-seq (E18.0 brain)
E13.5 brain (S1)
E13.5 brain (S2)
E15.5 brain (S1)
E15.5 brain (S2)
E18.5 brain (S1)
E18.5 brain (S2)
e
TSS Enrichment
f
Percentage of Fragments
Fragment Size (bp)
g
Normalized Insertion Profile
Distance From Center (bp)
h
ENCODE bulk ATAC (E15.5 Forebrain)
Aggregate Spatial ATAC (E15.5 Brain)
Spatial ATAC (E15.5 Brain) (300 grids)
Gene Track
Chd4
Nop2
Iffo1
Gapdh
Ncapd2
Scarna10
Mrpl51
Mir3098
Vamp1
i
UMIs per grid
DBiT-seq (E11.0 50μm)
j
Genes per grid
k
ENCODE bulk ATAC (E15.5 Brain)
Aggregate Spatial ATAC (E15.5 Brain)
Aggregate Spatial RNA (E15.5 Brain)
Gene Track
Actb

Fig. 2

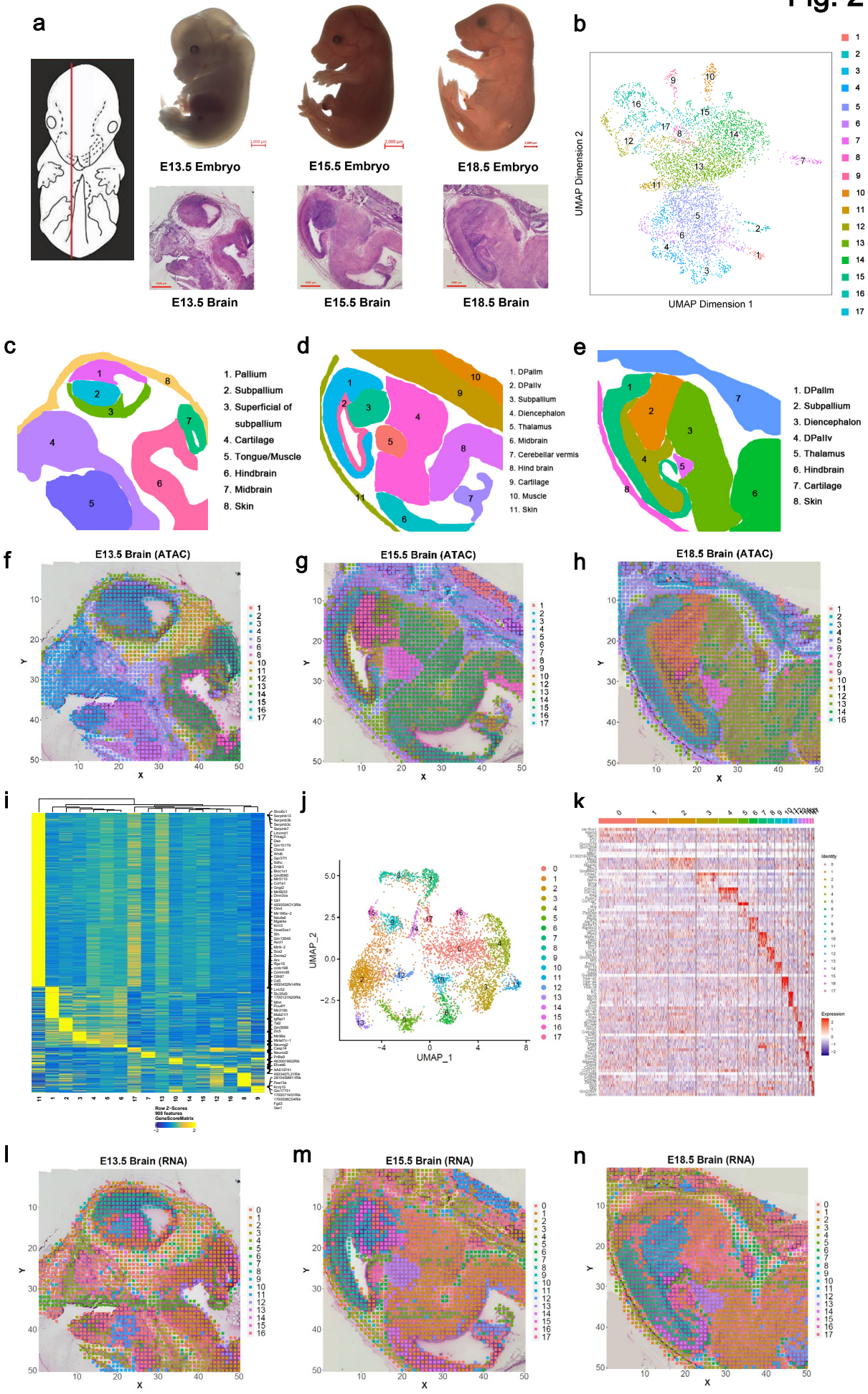
a
E13.5 Embryo
E15.5 Embryo
E18.5 Embryo
E13.5 Brain
E15.5 Brain
E18.5 Brain
b
UMAP Dimension 1
UMAP Dimension 2
c
1. Pallium
2. Subpallium
3. Superficial of subpallium
4. Cartilage
5. Tongue/Muscle
6. Hindbrain
7. Midbrain
8. Skin
d
1. DPallm
2. DPallv
3. Subpallium
4. Diencephalon
5. Thalamus
6. Midbrain
7. Cerebellar vermis
8. Hind brain
9. Cartilage
10. Muscle
11. Skin
e
1. DPallm
2. Subpallium
3. Diencephalon
4. DPallv
5. Thalamus
6. Hindbrain
7. Cartilage
8. Skin
f
E13.5 Brain (ATAC)
g
E15.5 Brain (ATAC)
h
E18.5 Brain (ATAC)
i
Row Z-Scores
908 features
GeneScoreMatrix
j
UMAP_1
UMAP_2
k
Identity
Expression
l
E13.5 Brain (RNA)
m
E15.5 Brain (RNA)
n
E18.5 Brain (RNA)

Fig. 3

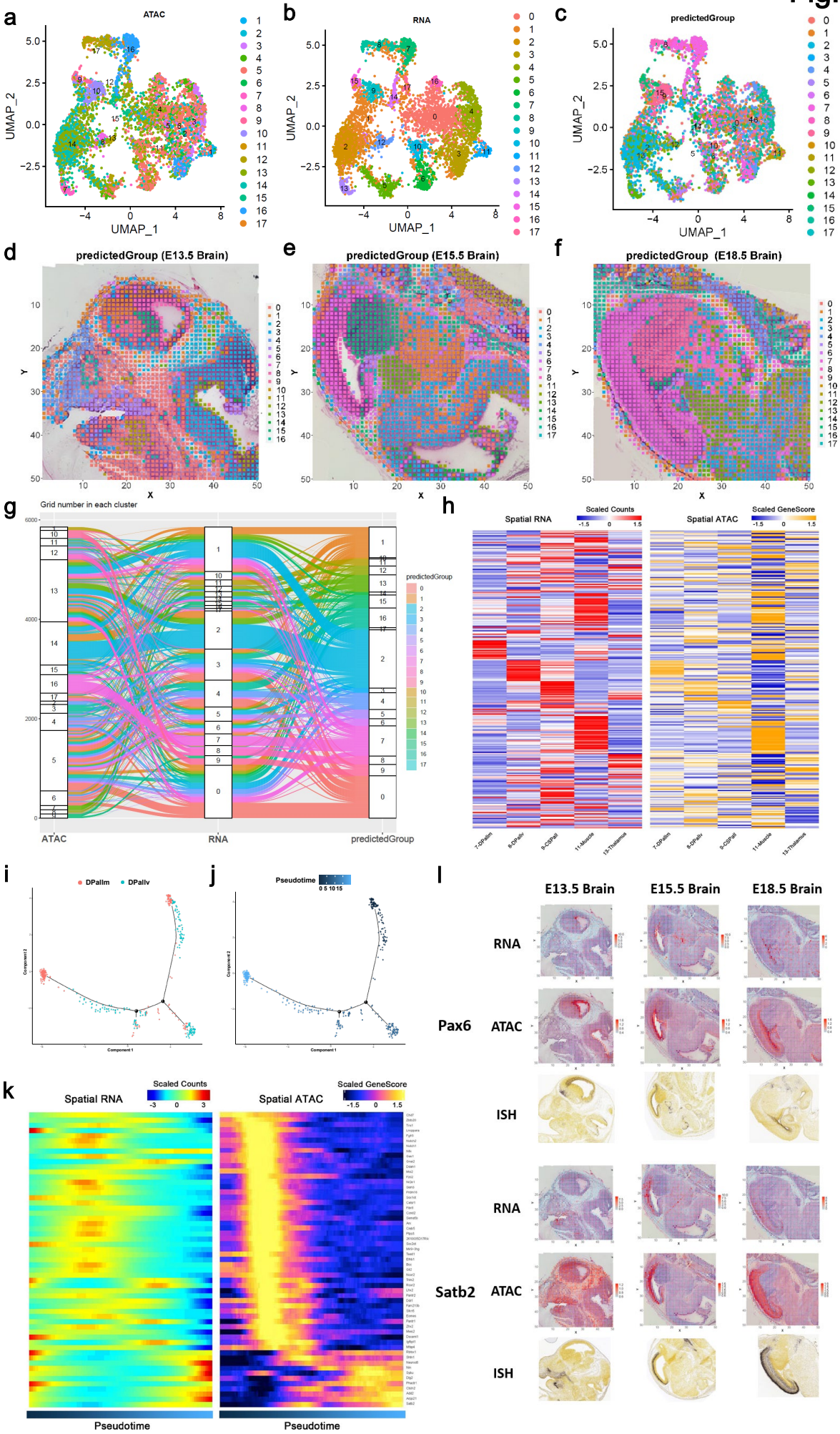
a
ATAC
UMAP_1
UMAP_2
b
RNA
c
predictedGroup
d
predictedGroup (E13.5 Brain)
e
predictedGroup (E15.5 Brain)
f
predictedGroup (E18.5 Brain)
g
Grid number in each cluster
ATAC
RNA
predictedGroup
h
Spatial RNA
Scaled Counts
Spatial ATAC
Scaled GeneScore
7-DPallm
8-DPallv
9-CSPall
11-Muscle
13-Thalamus
i
DPallm
DPallv
j
Pseudotime
k
Spatial RNA
Scaled Counts
Spatial ATAC
Scaled GeneScore
Pseudotime
l
E13.5 Brain
E15.5 Brain
E18.5 Brain
RNA
Pax6
ATAC
ISH
RNA
Satb2
ATAC
ISH

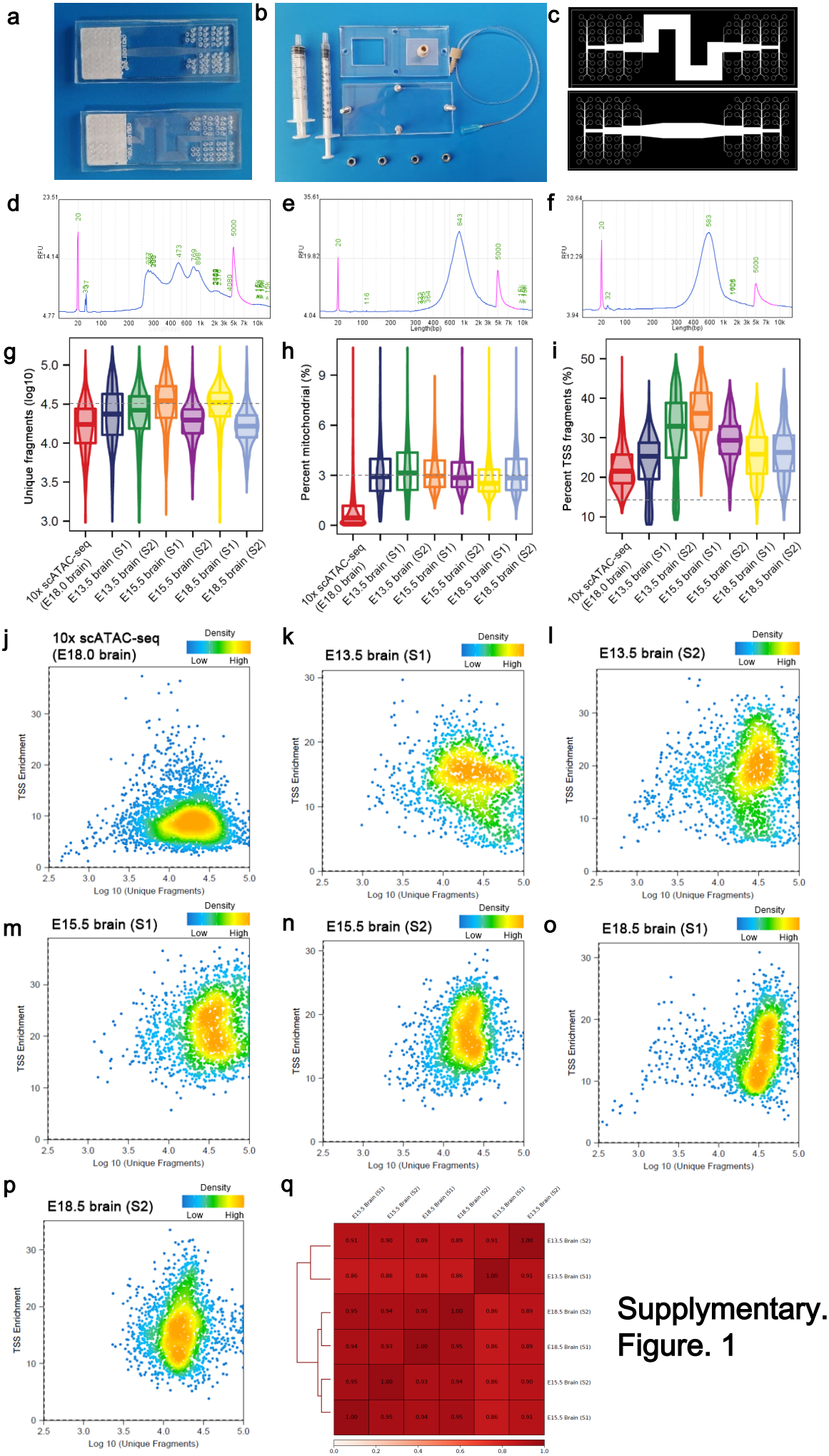

Supplymentary. Figure. 1

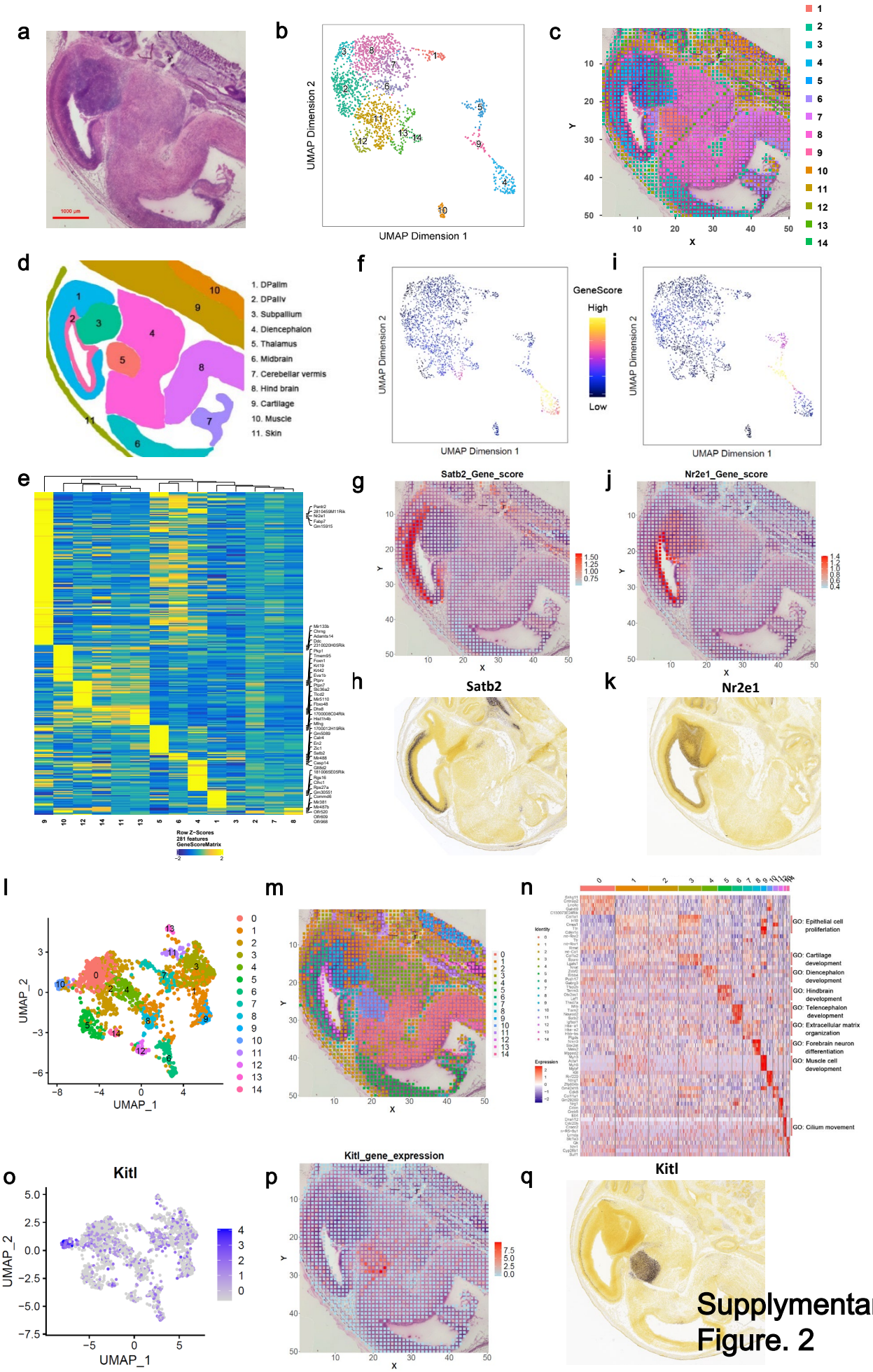

Supplymentary. Figure. 2

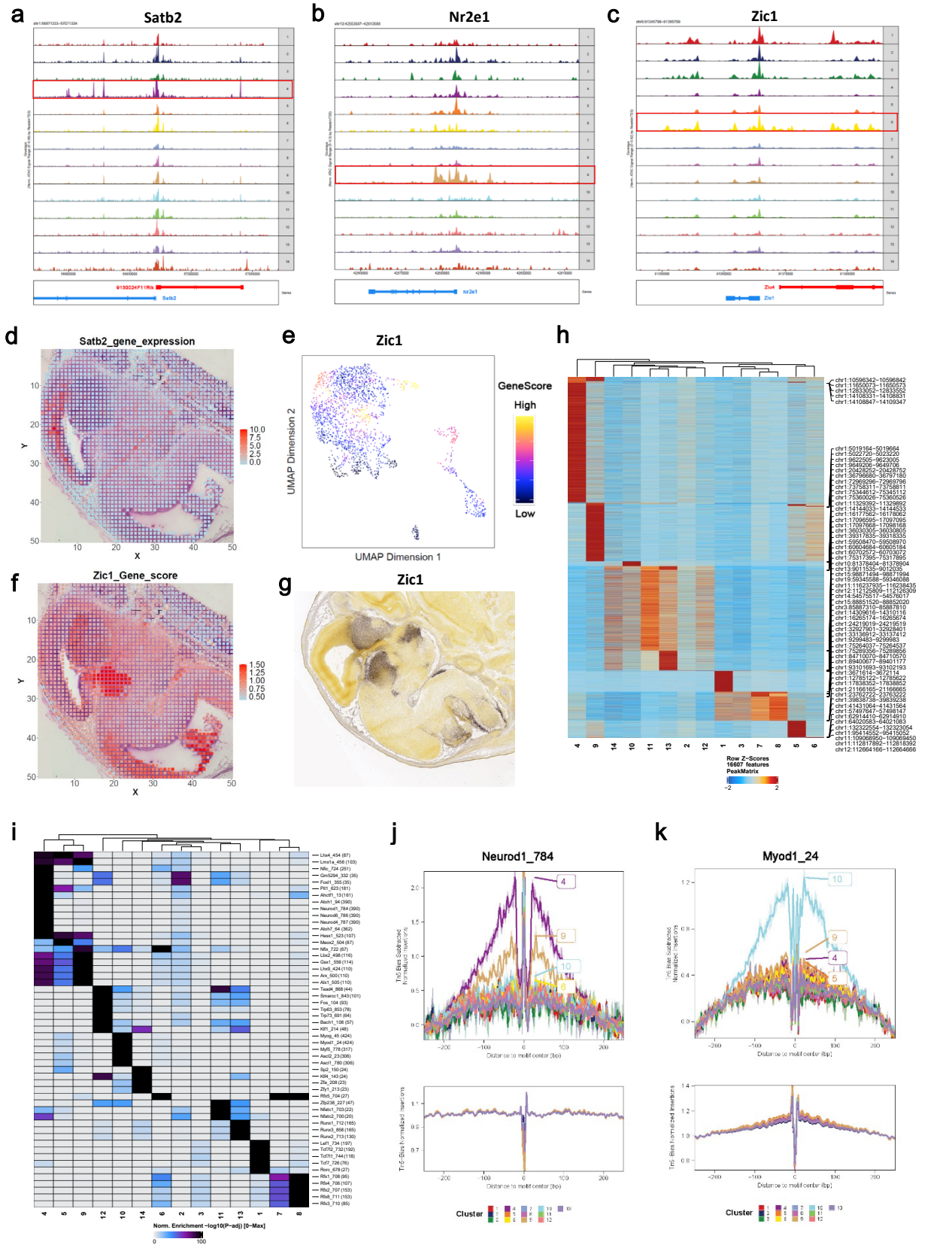

Supplymentary. Figure. 3

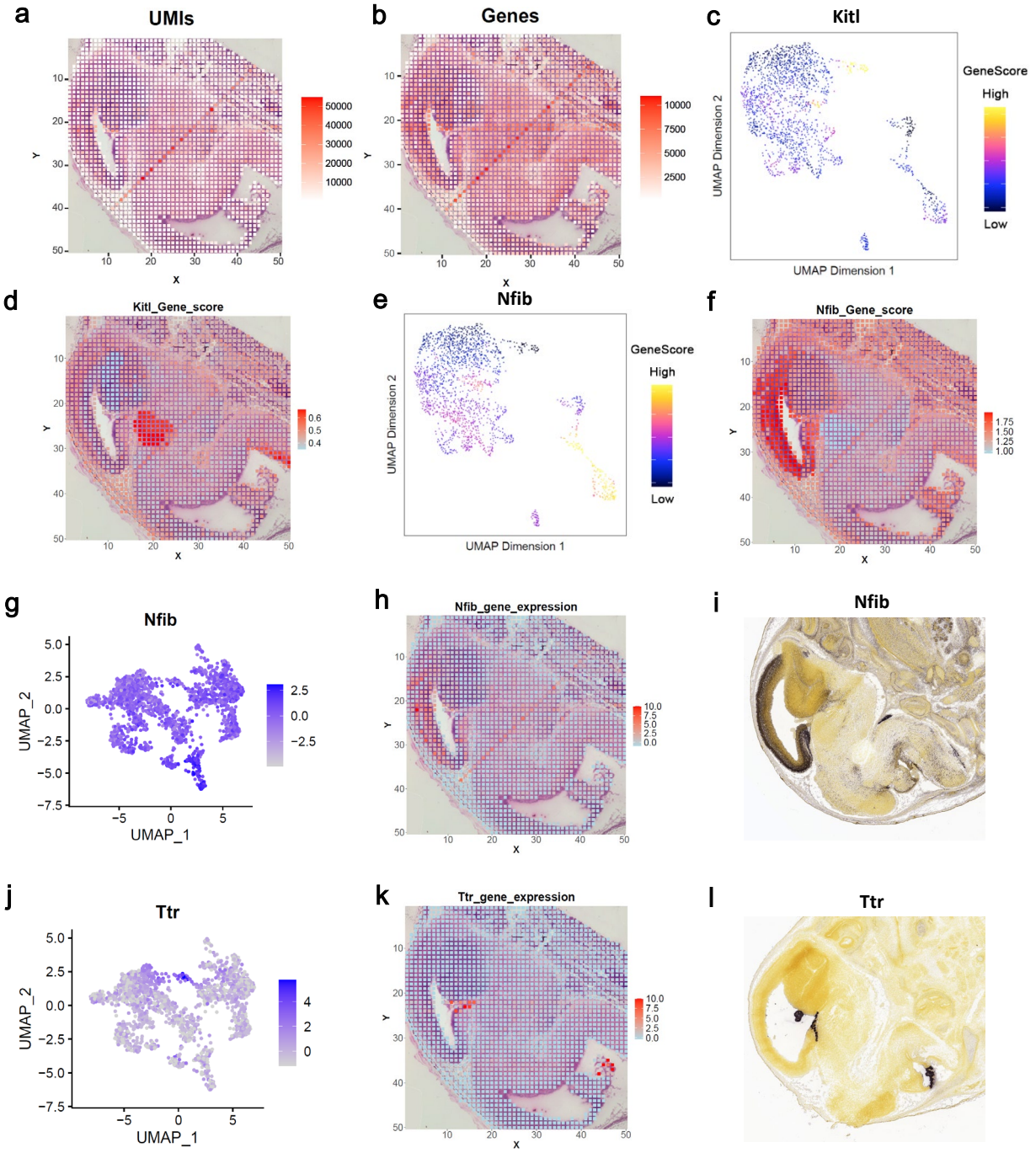

Supplymentary. Figure. 4

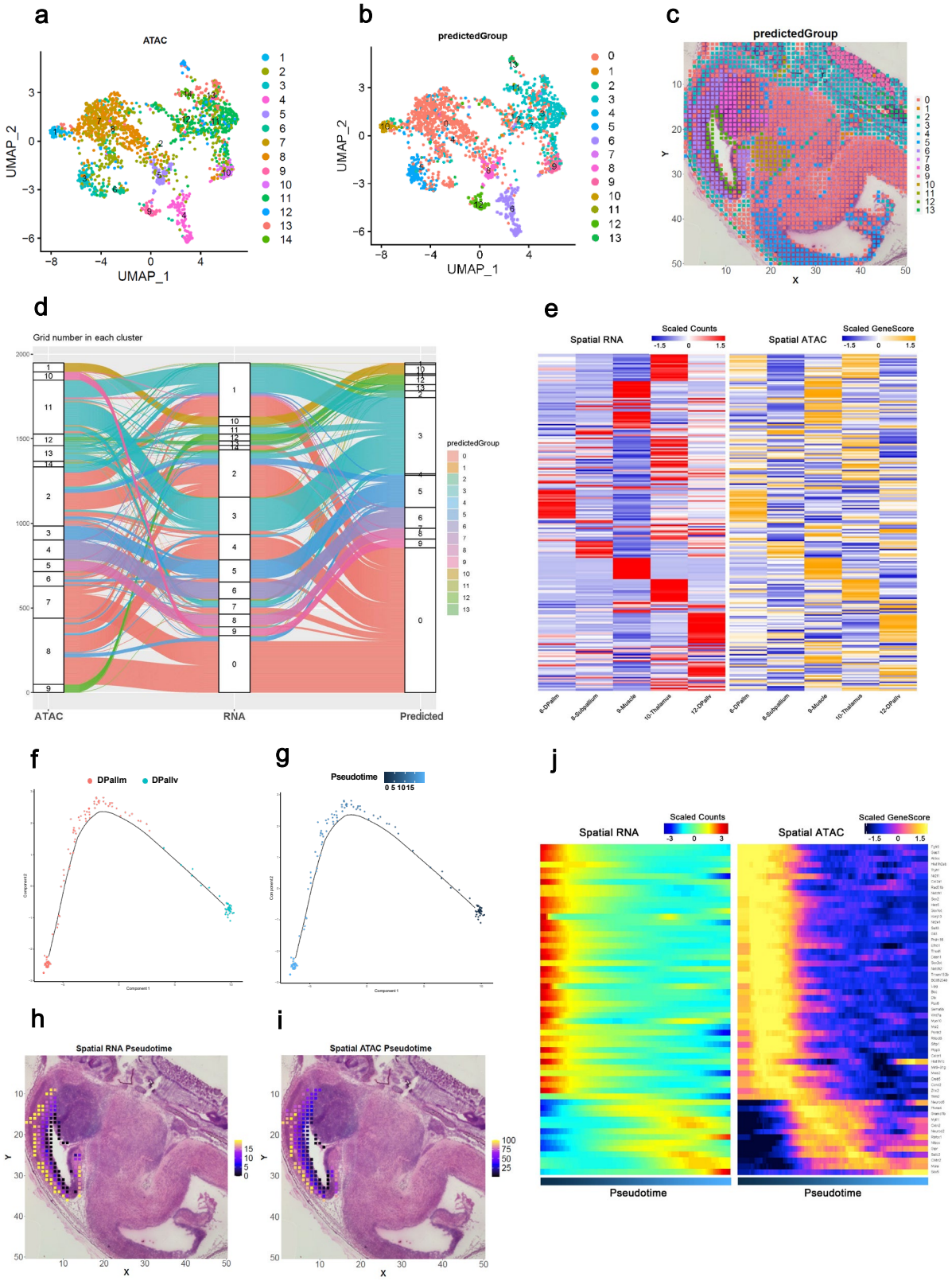

Supplymentary. Figure. 5

Section2

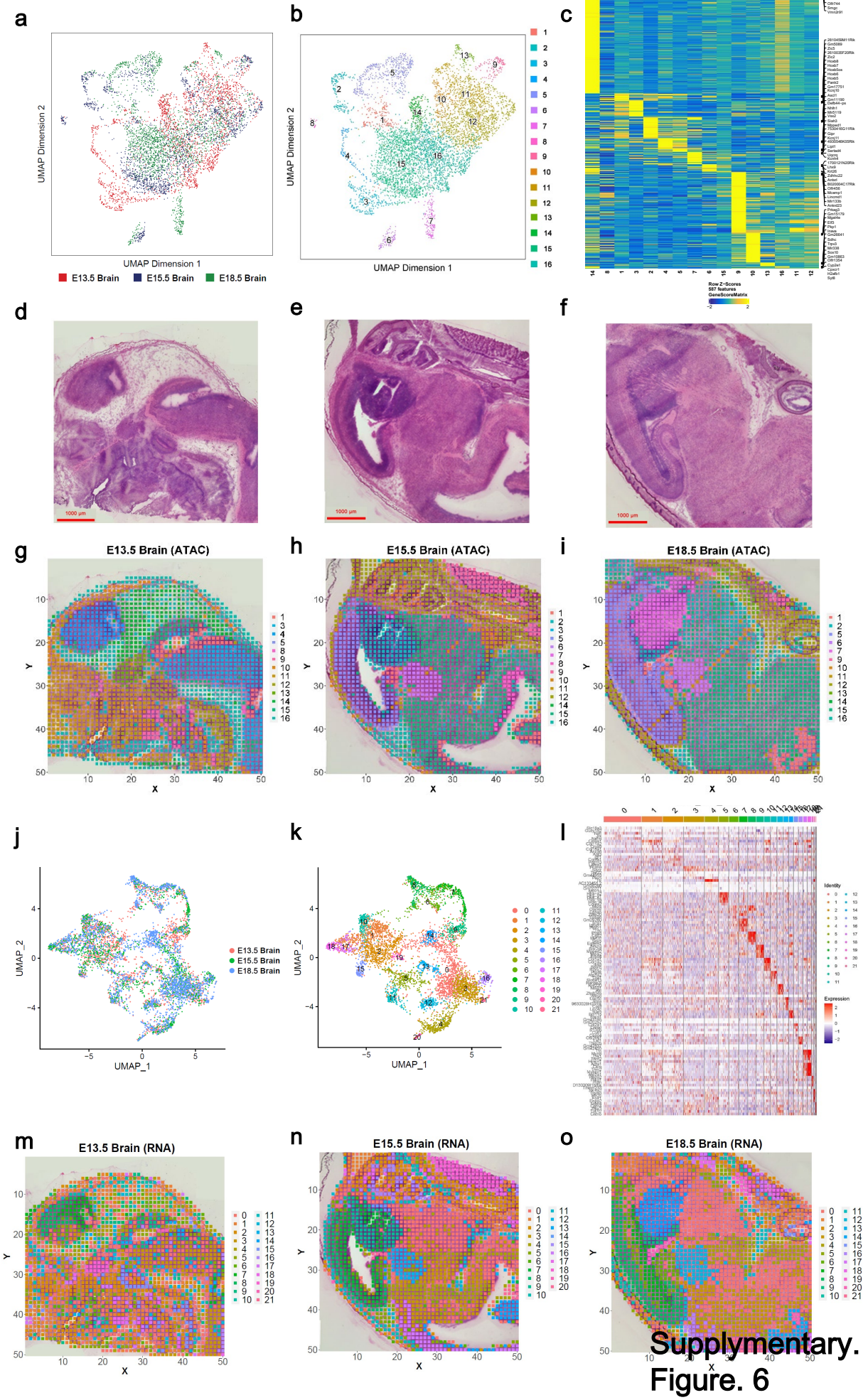

Supplymentary. Figure. 6

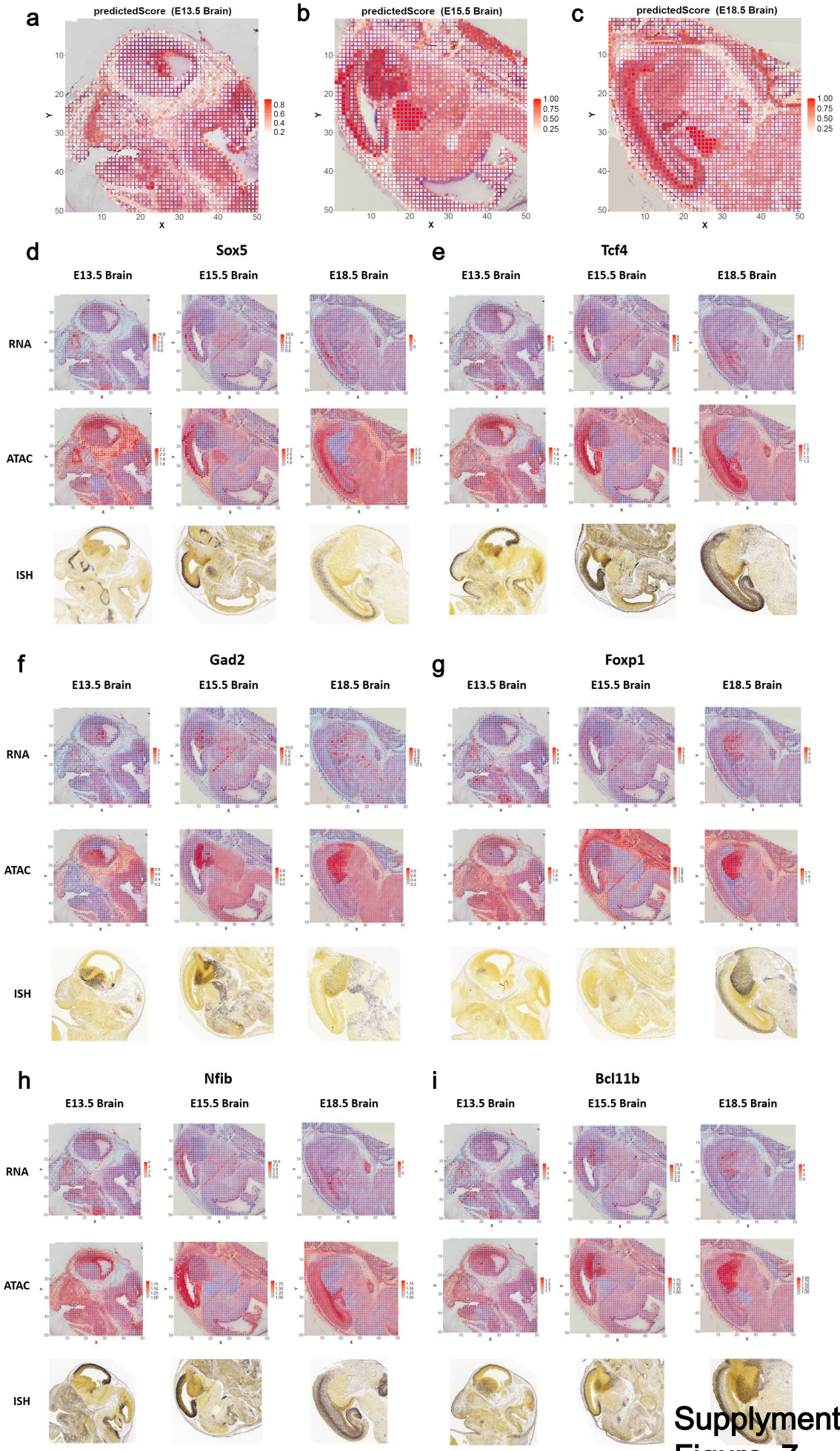

Supplymentary. Figure. 7

Table S1.

Name	**Sequence (5’ → 3’)**
Round 1 linker	CCGAGCCCACGAGACTCGGACGATCATGGG
Round 2 linker	CAAGTATGCAGCGCGCGAAACATCGGCCAC
RT_primer	/5Phos/GTCTCGTGGGCTCGGAGATGTGTATAAGAGACAG NNNNNNNNNN/iBiodT/TTTTTTTTTTTTTTVN
TSO_0127	AAGCAGTGGTATCAACGCAGAGTGAATrGrG+G
BC-0108	AAGCAGTGGTATCAACGCAGAGT
P7	CAAGCAGAAGACGGCATACGAGAT
Ad1.01	AATGATACGGCGACCACCGAGATCTACACTAGATCGCTC GTCGGCAGCGTCAGATGTGTAT
Ad1.02	AATGATACGGCGACCACCGAGATCTACACCTCTCTATTC GTCGGCAGCGTCAGATGTGTAT
Ad1.03	AATGATACGGCGACCACCGAGATCTACACTATCCTCTTC GTCGGCAGCGTCAGATGTGTAT
Ad1.04	AATGATACGGCGACCACCGAGATCTACACAGAGTAGATC GTCGGCAGCGTCAGATGTGTAT
Ad1.05	AATGATACGGCGACCACCGAGATCTACACGTAAGGAGTC GTCGGCAGCGTCAGATGTGTAT
Ad1.06	AATGATACGGCGACCACCGAGATCTACACACTGCATATC GTCGGCAGCGTCAGATGTGTAT
Ad1.07	AATGATACGGCGACCACCGAGATCTACACAAGGAGTATC GTCGGCAGCGTCAGATGTGTAT
Ad1.08	AATGATACGGCGACCACCGAGATCTACACCTAAGCCTTC GTCGGCAGCGTCAGATGTGTAT

Table S2.

Name	Sequence
Round1 barcodes	
Round1_01	/5Phos/CGCGCTGCATACTTGTCCTACCAGTCCCATGATCGTCCGA
Round1_02	/5Phos/CGCGCTGCATACTTGGCGTTGGAGCCCCATGATCGTCCGA
Round1_03	/5Phos/CGCGCTGCATACTTGGATCTTACGCCCCATGATCGTCCGA
Round1_04	/5Phos/CGCGCTGCATACTTGCTGATGGTCACCCATGATCGTCCGA
Round1_05	/5Phos/CGCGCTGCATACTTGCCGAGAATCCCCCATGATCGTCCGA
Round1_06	/5Phos/CGCGCTGCATACTTGGCCGCAACGACCCATGATCGTCCGA
Round1_07	/5Phos/CGCGCTGCATACTTGTGAGTCTGGCCCCATGATCGTCCGA
Round1_08	/5Phos/CGCGCTGCATACTTGTGCGGACCTACCCATGATCGTCCGA
Round1_09	/5Phos/CGCGCTGCATACTTGACGGAGGCGGCCCATGATCGTCCGA
Round1_10	/5Phos/CGCGCTGCATACTTGTAGATCTACTCCCATGATCGTCCGA
Round1_11	/5Phos/CGCGCTGCATACTTGAATTAAGACTCCCATGATCGTCCGA
Round1_12	/5Phos/CGCGCTGCATACTTGTTATTCATTCCCCATGATCGTCCGA
Round1_13	/5Phos/CGCGCTGCATACTTGTTGACTTCAGCCCATGATCGTCCGA
Round1_14	/5Phos/CGCGCTGCATACTTGAGAGCTATAACCCATGATCGTCCGA
Round1_15	/5Phos/CGCGCTGCATACTTGCTAAGAGAAGCCCATGATCGTCCGA
Round1_16	/5Phos/CGCGCTGCATACTTGACTCAATAGGCCCATGATCGTCCGA
Round1_17	/5Phos/CGCGCTGCATACTTGCTTGCGCCGCCCCATGATCGTCCGA
Round1_18	/5Phos/CGCGCTGCATACTTGGGTACTGCCTCCCATGATCGTCCGA
Round1_19	/5Phos/CGCGCTGCATACTTGTAGAATTAACCCCATGATCGTCCGA
Round1_20	/5Phos/CGCGCTGCATACTTGGCCATTCTCCCCCATGATCGTCCGA

Round1_21	/5Phos/CGCGCTGCATACTTGTGCCGGCAGACCCATGATCGTCCGA
Round1_22	/5Phos/CGCGCTGCATACTTGTTACCGAGGCCCCATGATCGTCCGA
Round1_23	/5Phos/CGCGCTGCATACTTGATCATATTAGCCCATGATCGTCCGA
Round1_24	/5Phos/CGCGCTGCATACTTGTGGTCAGCCACCCATGATCGTCCGA
Round1_25	/5Phos/CGCGCTGCATACTTGACTATGCAATCCCATGATCGTCCGA
Round1_26	/5Phos/CGCGCTGCATACTTGCGACGCGACTCCCATGATCGTCCGA
Round1_27	/5Phos/CGCGCTGCATACTTGGATACGGAACCCCATGATCGTCCGA
Round1_28	/5Phos/CGCGCTGCATACTTGTTATCCGGATCCCATGATCGTCCGA
Round1_29	/5Phos/CGCGCTGCATACTTGTAGAGTAATACCCATGATCGTCCGA
Round1_30	/5Phos/CGCGCTGCATACTTGGCAGGTCCGTCCCATGATCGTCCGA
Round1_31	/5Phos/CGCGCTGCATACTTGTCGGCCTTACCCCATGATCGTCCGA
Round1_32	/5Phos/CGCGCTGCATACTTGAGAACGTCTCCCCATGATCGTCCGA
Round1_33	/5Phos/CGCGCTGCATACTTGCCAGTTCCAACCCATGATCGTCCGA
Round1_34	/5Phos/CGCGCTGCATACTTGACTTAACCTTCCCATGATCGTCCGA
Round1_35	/5Phos/CGCGCTGCATACTTGCAACCGCTAACCCATGATCGTCCGA
Round1_36	/5Phos/CGCGCTGCATACTTGGACCTTGATACCCATGATCGTCCGA
Round1_37	/5Phos/CGCGCTGCATACTTGTCTGATACCACCCATGATCGTCCGA
Round1_38	/5Phos/CGCGCTGCATACTTGGAAGATCGAGCCCATGATCGTCCGA
Round1_39	/5Phos/CGCGCTGCATACTTGAAGAAGCTAGCCCATGATCGTCCGA
Round1_40	/5Phos/CGCGCTGCATACTTGTCCGGCCTCGCCCATGATCGTCCGA
Round1_41	/5Phos/CGCGCTGCATACTTGAGAGAAGGTTCCCATGATCGTCCGA
Round1_42	/5Phos/CGCGCTGCATACTTGCATACTCCGACCCATGATCGTCCGA

Round1_43	/5Phos/CGCGCTGCATACTTGGCTAACTTGCCCCATGATCGTCCGA
Round1_44	/5Phos/CGCGCTGCATACTTGGGCTGAGCTCCCCATGATCGTCCGA
Round1_45	/5Phos/CGCGCTGCATACTTGCCGATTCCTGCCCATGATCGTCCGA
Round1_46	/5Phos/CGCGCTGCATACTTGACCGCCAACCCCCATGATCGTCCGA
Round1_47	/5Phos/CGCGCTGCATACTTGATAAGGAGCACCCATGATCGTCCGA
Round1_48	/5Phos/CGCGCTGCATACTTGCGAACGCCGGCCCATGATCGTCCGA
Round1_49	/5Phos/CGCGCTGCATACTTGGGTATGCTTGCCCATGATCGTCCGA
Round1_50	/5Phos/CGCGCTGCATACTTGAACCTGCGTACCCATGATCGTCCGA
Round2 barcodes	
Round2_01	CAAGCAGAAGACGGCATACGAGATTCCTACCAGTGTGGCCGATGTTTCG
Round2_02	CAAGCAGAAGACGGCATACGAGATGCGTTGGAGCGTGGCCGATGTTTCG
Round2_03	CAAGCAGAAGACGGCATACGAGATGATCTTACGCGTGGCCGATGTTTCG
Round2_04	CAAGCAGAAGACGGCATACGAGATCTGATGGTCAGTGGCCGATGTTTCG
Round2_05	CAAGCAGAAGACGGCATACGAGATCCGAGAATCCGTGGCCGATGTTTCG
Round2_06	CAAGCAGAAGACGGCATACGAGATGCCGCAACGAGTGGCCGATGTTTCG
Round2_07	CAAGCAGAAGACGGCATACGAGATTGAGTCTGGCGTGGCCGATGTTTCG
Round2_08	CAAGCAGAAGACGGCATACGAGATTGCGGACCTAGTGGCCGATGTTTCG
Round2_09	CAAGCAGAAGACGGCATACGAGATACGGAGGCGGGTGGCCGATGTTTCG
Round2_10	CAAGCAGAAGACGGCATACGAGATTAGATCTACTGTGGCCGATGTTTCG
Round2_11	CAAGCAGAAGACGGCATACGAGATAATTAAGACTGTGGCCGATGTTTCG
Round2_12	CAAGCAGAAGACGGCATACGAGATTTATTCATTCGTGGCCGATGTTTCG
Round2_13	CAAGCAGAAGACGGCATACGAGATTTGACTTCAGGTGGCCGATGTTTCG

Round2_14	CAAGCAGAAGACGGCATACGAGATAGAGCTATAAGTGGCCGATGTTTCG
Round2_15	CAAGCAGAAGACGGCATACGAGATCTAAGAGAAGGTGGCCGATGTTTCG
Round2_16	CAAGCAGAAGACGGCATACGAGATACTCAATAGGGTGGCCGATGTTTCG
Round2_17	CAAGCAGAAGACGGCATACGAGATCTTGCGCCGCGTGGCCGATGTTTCG
Round2_18	CAAGCAGAAGACGGCATACGAGATGGTACTGCCTGTGGCCGATGTTTCG
Round2_19	CAAGCAGAAGACGGCATACGAGATTAGAATTAACGTGGCCGATGTTTCG
Round2_20	CAAGCAGAAGACGGCATACGAGATGCCATTCTCCGTGGCCGATGTTTCG
Round2_21	CAAGCAGAAGACGGCATACGAGATTGCCGGCAGAGTGGCCGATGTTTCG
Round2_22	CAAGCAGAAGACGGCATACGAGATTTACCGAGGCGTGGCCGATGTTTCG
Round2_23	CAAGCAGAAGACGGCATACGAGATATCATATTAGGTGGCCGATGTTTCG
Round2_24	CAAGCAGAAGACGGCATACGAGATTGGTCAGCCAGTGGCCGATGTTTCG
Round2_25	CAAGCAGAAGACGGCATACGAGATACTATGCAATGTGGCCGATGTTTCG
Round2_26	CAAGCAGAAGACGGCATACGAGATCGACGCGACTGTGGCCGATGTTTCG
Round2_27	CAAGCAGAAGACGGCATACGAGATGATACGGAACGTGGCCGATGTTTCG
Round2_28	CAAGCAGAAGACGGCATACGAGATTTATCCGGATGTGGCCGATGTTTCG
Round2_29	CAAGCAGAAGACGGCATACGAGATTAGAGTAATAGTGGCCGATGTTTCG
Round2_30	CAAGCAGAAGACGGCATACGAGATGCAGGTCCGTGTGGCCGATGTTTCG
Round2_31	CAAGCAGAAGACGGCATACGAGATTCGGCCTTACGTGGCCGATGTTTCG
Round2_32	CAAGCAGAAGACGGCATACGAGATAGAACGTCTCGTGGCCGATGTTTCG
Round2_33	CAAGCAGAAGACGGCATACGAGATCCAGTTCCAAGTGGCCGATGTTTCG
Round2_34	CAAGCAGAAGACGGCATACGAGATACTTAACCTTGTGGCCGATGTTTCG
Round2_35	CAAGCAGAAGACGGCATACGAGATCAACCGCTAAGTGGCCGATGTTTCG

Round2_36	CAAGCAGAAGACGGCATACGAGATGACCTTGATAGTGGCCGATGTTTCG
Round2_37	CAAGCAGAAGACGGCATACGAGATTCTGATACCAGTGGCCGATGTTTCG
Round2_38	CAAGCAGAAGACGGCATACGAGATGAAGATCGAGGTGGCCGATGTTTCG
Round2_39	CAAGCAGAAGACGGCATACGAGATAAGAAGCTAGGTGGCCGATGTTTCG
Round2_40	CAAGCAGAAGACGGCATACGAGATTCCGGCCTCGGTGGCCGATGTTTCG
Round2_41	CAAGCAGAAGACGGCATACGAGATAGAGAAGGTTGTGGCCGATGTTTCG
Round2_42	CAAGCAGAAGACGGCATACGAGATCATACTCCGAGTGGCCGATGTTTCG
Round2_43	CAAGCAGAAGACGGCATACGAGATGCTAACTTGCGTGGCCGATGTTTCG
Round2_44	CAAGCAGAAGACGGCATACGAGATGGCTGAGCTCGTGGCCGATGTTTCG
Round2_45	CAAGCAGAAGACGGCATACGAGATCCGATTCCTGGTGGCCGATGTTTCG
Round2_46	CAAGCAGAAGACGGCATACGAGATACCGCCAACCGTGGCCGATGTTTCG
Round2_47	CAAGCAGAAGACGGCATACGAGATATAAGGAGCAGTGGCCGATGTTTCG
Round2_48	CAAGCAGAAGACGGCATACGAGATCGAACGCCGGGTGGCCGATGTTTCG
Round2_49	CAAGCAGAAGACGGCATACGAGATGGTATGCTTGGTGGCCGATGTTTCG
Round2_50	CAAGCAGAAGACGGCATACGAGATAACCTGCGTAGTGGCCGATGTTTCG